

Communications Infrastructure
for the
MOST Microsatellite Project
(excerpt)

Laura Halliday

Copyright © 2000, Laura Halliday.
This excerpt from my thesis is provided for your information and interest.
Kindly check with me before redistributing it.

7.4 Telemetry analysis

Telemetry was downloaded from satellites and analyzed. The results illustrate many of the issues involved in the design, construction and operation of a satellite.

The whole orbit data results presented in this section were downloaded in encoded format from TO–31 and UO–22 in the formats described in Sections 4.3.1 and 4.3.3. They were decoded with the display program vbt1m described in Appendix C.2, producing comma-delimited text files which were then imported into Microsoft Excel to produce the plots presented here.

A whole orbit data survey was obtained from AO–16 in the format described in Section 4.3.4 and is presented here. Other analyses presented here cover task messages and log files.

7.4.1 Whole orbit data: TO–31

The results presented in Figures 7.6 to 7.9 were produced by decoding a TO–31 whole-orbit data file that covers satellite activity from 1200 UTC to 2359 UTC on 28 November 1999.

Figure 7.6 clearly shows the thermal environment of the spacecraft. The alternation of sun and eclipse is clearly visible in the temperature excursions of the solar panels, which heat to 25C in the sun, then cool to -35C during eclipses. This cycle occurs every orbit, approximately every 100 minutes for TO–31. Inside the spacecraft the batteries and electronics experience a comfortable room-temperature environment with only modest temperature variations.

TO–31 derives its electrical power from solar cells which charge the on-board batteries. Figure 7.7 shows a clear alternation of charge and discharge cycles, charging when the spacecraft is in the sun, and discharging during eclipses. On exit from eclipse the top priority of the power system is to recharge the batteries, accounting for the initial surge over 2 amperes. Once the batteries are recharged the current falls to a 200 mA maintenance level.

The 500mA spikes at 1805 and 1924 UTC correlate with magnetic anomalies at the same time, as illustrated in Figure 7.9. However, the relationship may be entirely coincidental: other spikes in other telemetry files do not correspond with magnetic activity.

The solar cells on TO–31 generate electricity when the spacecraft is in the sun, and cease to do so during eclipses. This is clear from Figure 7.8, which shows that the voltage from the solar arrays rises to over 40 volts in the sun, but drops to the battery voltage (nominally 12 volts) during eclipse.

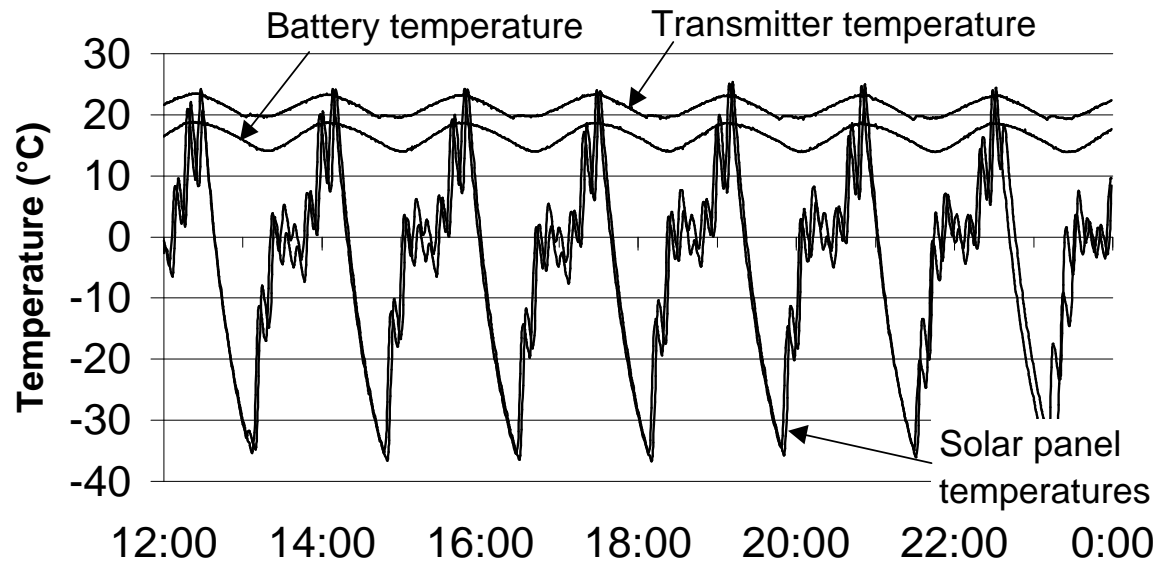


Figure 7.6: TO-31 temperatures: 1200–2359 UTC 28 November 1999

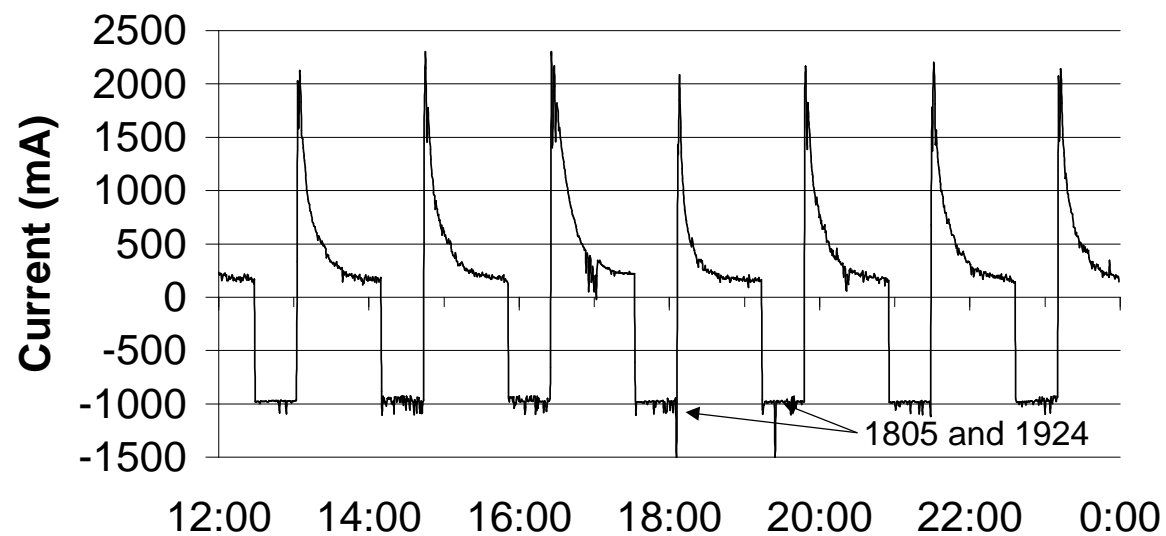


Figure 7.7: TO-31 battery current: 1200–2359 UTC 28 November 1999

The battery voltage shows small variations during this period, reflecting the charge/discharge cycle of the spacecraft.

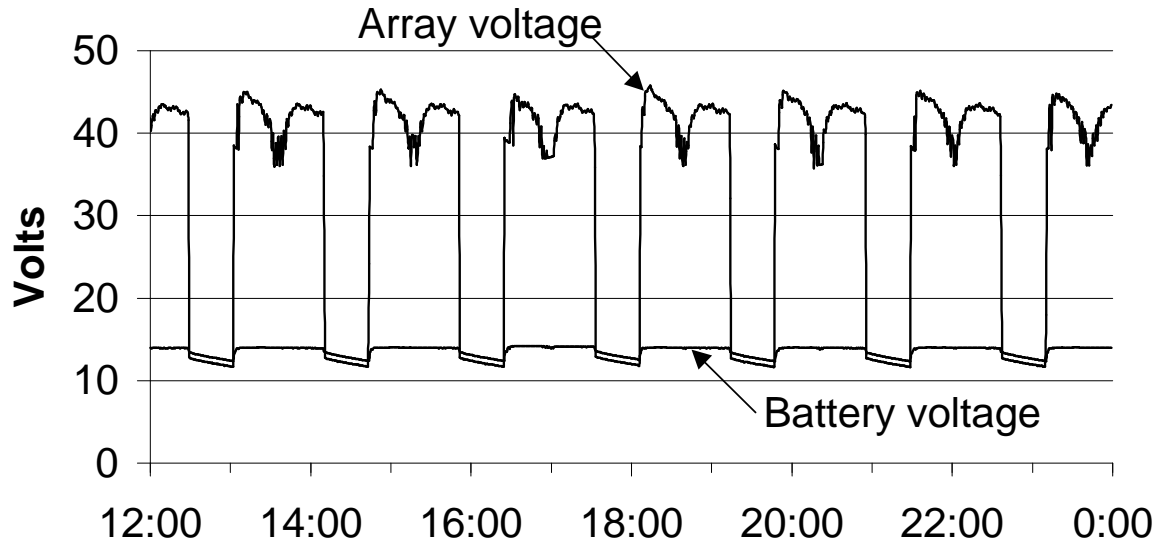


Figure 7.8: TO-31 voltages: 1200–2359 UTC 28 November 1999

Like all the satellites built by the University of Surrey and related programs, TO-31 is stabilized with a gravity-gradient boom. The boom defines the spacecraft Z axis, and is the axis of the spacecraft spin. This is clear from the readings of the spacecraft magnetometers presented in Figure 7.9. The rapid variation on the X and Y magnetometers is due to the spacecraft spinning every 10 minutes. The slow variation on the Z magnetometer is caused by the orbit of the spacecraft altering the spacecraft's orientation to the Earth's magnetic field. There is an additional slower variation caused by the Earth's axial spin altering the relationship of the North and South Magnetic Poles with the spacecraft orbit. The large spikes in the magnetometer readings correlate with the large spikes in the power system seen in Figure 7.7, but may still be coincidental. Even if they are the result of a single phenomenon, it is unknown which is the cause and which is the effect.

7.4.2 Whole orbit data: UO-22

The analysis of UO-22 whole orbit data is facilitated by the unbroken availability of data for an extended period, from June to December 1999. By gathering data for an extended period it was hoped that seasonal changes could be detected in the spacecraft, with the possibility of detection of long-term changes as well. Long-term changes were observed in the spacecraft thermal environment

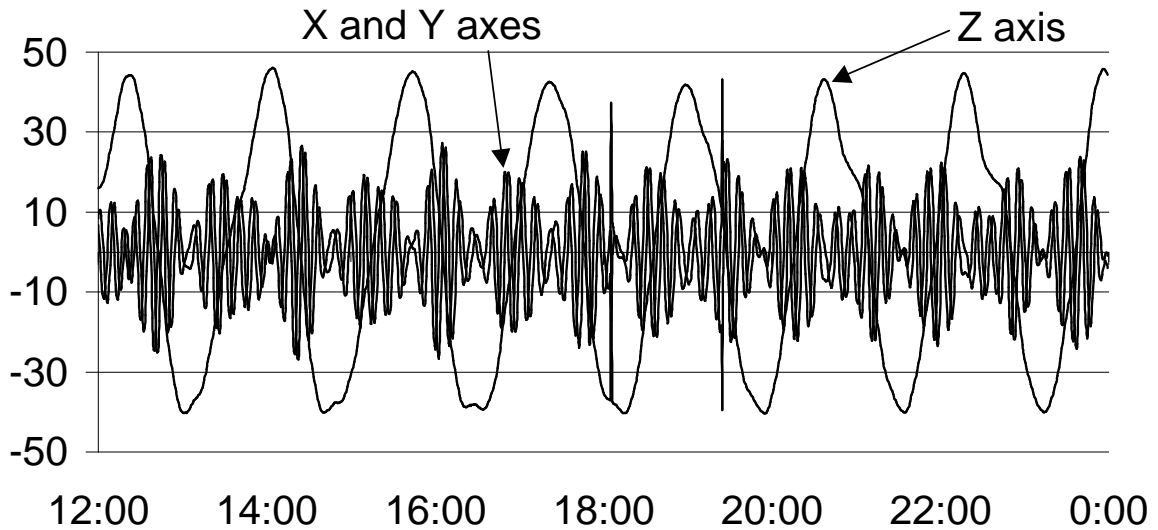


Figure 7.9: TO-31 magnetometers: 1200–2359 UTC 28 November 1999

which were initially believed to be seasonal, but have now been confirmed to be the result of orbital perturbations (3).

The thermal environment of UO-22 is illustrated in Figures 7.10 to 7.13 and shows temperature variations related to the cycle of sun and eclipses. The solar array temperatures are the subject of a detailed analysis conducted once per month; the internal temperatures are recorded continuously.

It is clear that the satellite is running hot, especially in November. Additional data were analyzed to isolate the cause.

The data in Figure 7.11 suggest an increasing trend, but the exact cause of the trend is unknown: the rise is much faster than the temperature change from July to November 1999.

UO-22 derives electrical power from solar arrays, which generate over 40 volts in the sun, but drop to the voltage of the battery, nominally 12 volts, in eclipses. This is clear in Figures 7.14 and 7.15. The eclipse period is clear, and its length may be estimated from the telemetry data: 26 minutes in July, but only 18 minutes at the end of November. The satellite has less time to cool each orbit, and thus runs hotter. The temperature variation may be estimated: to a first approximation, the energy input to the satellite is proportional to the time the spacecraft spends in the sun. From July to November this has increased from 74 minutes per orbit to 82 minutes per orbit, an increase of 10.8%. Absolute temperature varies as the fourth root of energy input (the Stefan-Boltzmann Equation) (4), and the fourth root of 1.108 is approximately 1.026, a 2.6% increase in absolute temperature. This

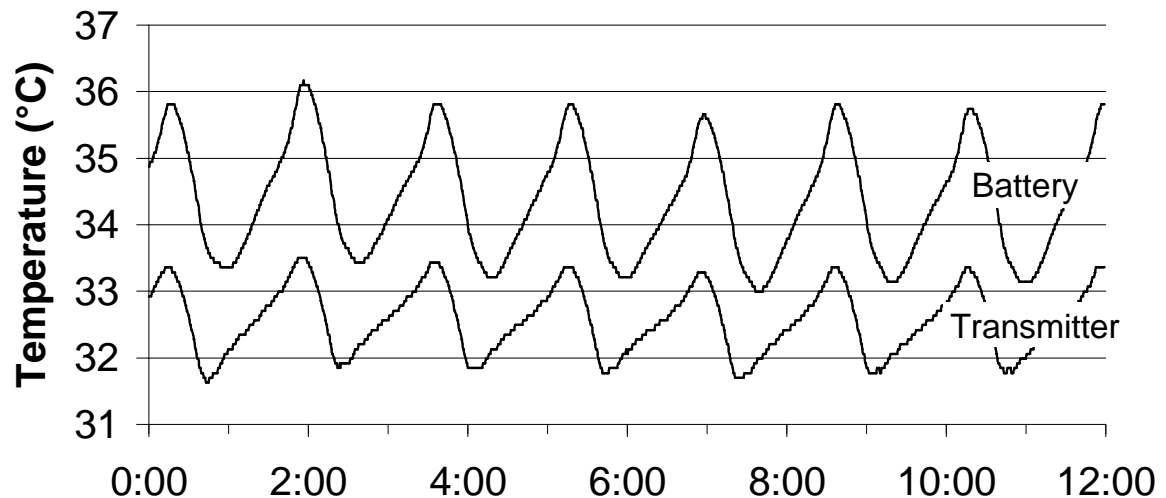


Figure 7.10: UO-22 internal temperatures: 0000–1159 UTC 6 July 1999

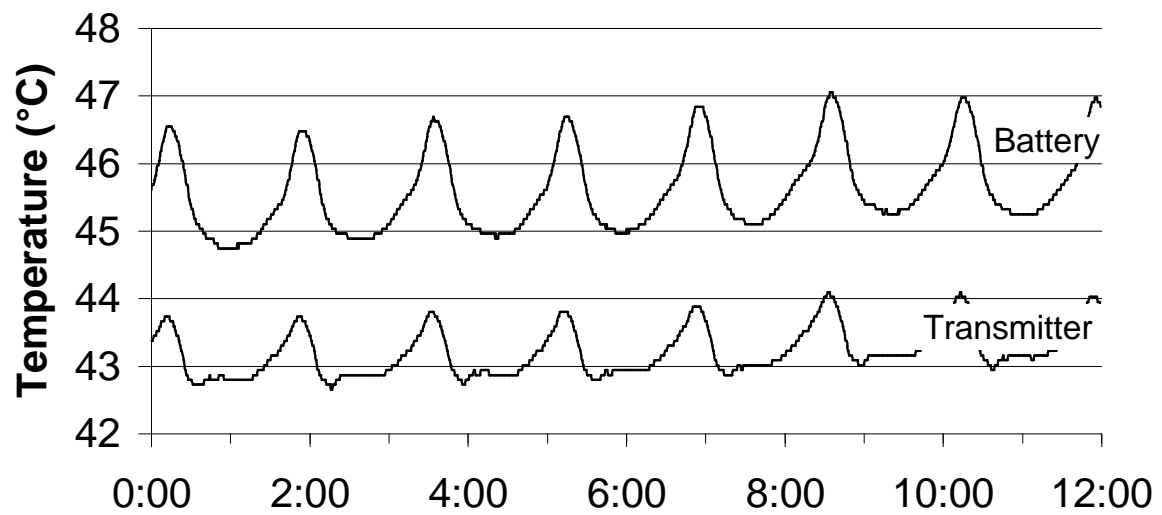


Figure 7.11: UO-22 internal temperatures: 0000–1159 UTC 26 November 1999

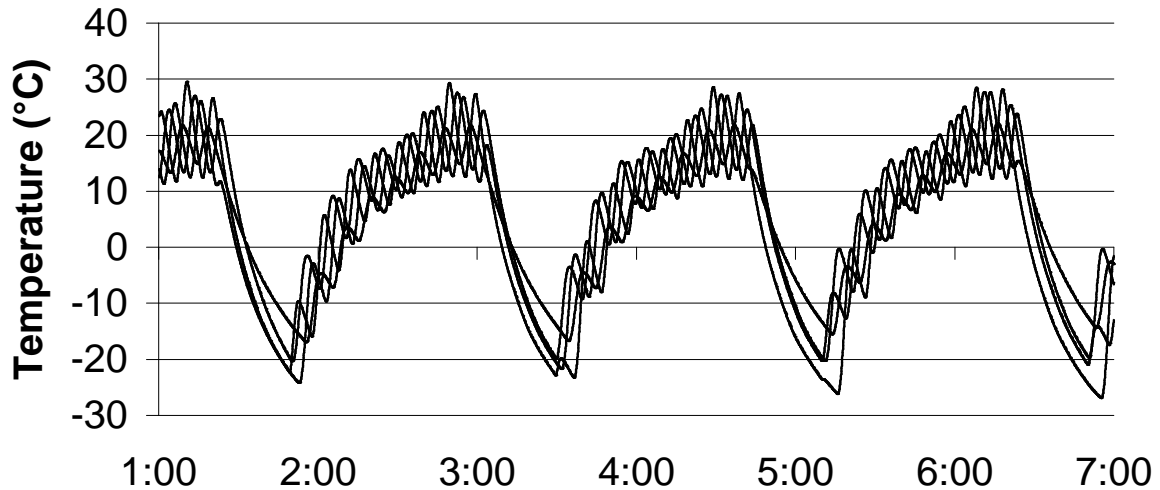


Figure 7.12: UO-22 solar array temperatures: 0100–0659 UTC 15 July 1999

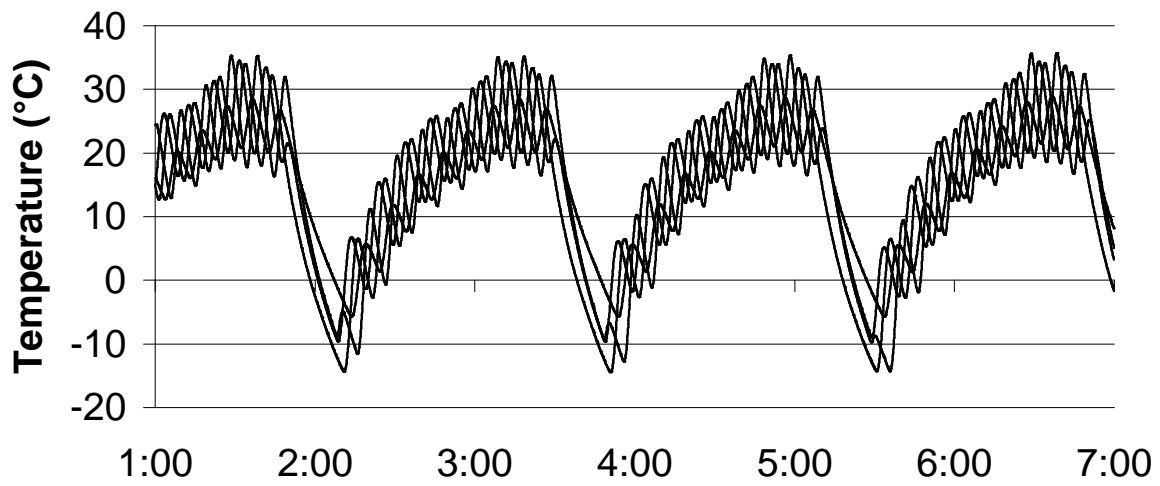


Figure 7.13: UO-22 solar array temperatures: 0100–0659 UTC 15 November 1999

corresponds to a temperature rise of approximately 8 degrees, close to the observed temperature increase. Such seasonal changes are to be expected in satellite operations, and must be allowed for in the thermal design.

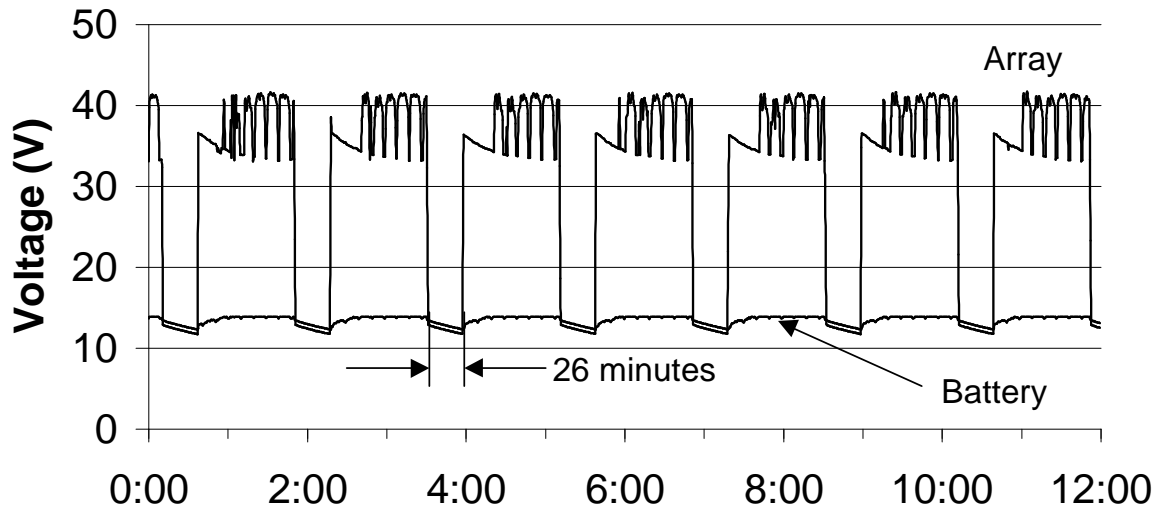


Figure 7.14: UO-22 solar array and battery voltages: 0000–1159 UTC 6 July 1999

December whole orbit data show a further increase in temperature to 47 C, with the eclipse period down to 15 minutes.

Other activities of the satellite may be observed by analysis of whole orbit data. Figures 7.16 and 7.17 show a clear cycle of charging while in the sun and discharging during eclipses. While there are no gross differences between the seasons, it is probable that more detailed analysis of the data would show a drop in charging efficiency with higher battery temperature.

Like TO-31, UO-22 shows spikes in battery current. The magnetometer data in Figures 7.18 and 7.19 do not correlate with the spikes, which are thus not related to magnetorquer activity. The data show the 10 minute spin of the spacecraft, the spacecraft orbit around the Earth's magnetic field, and the varying orientation of the spacecraft with respect to the magnetic poles as the Earth rotates. Like TO-31, UO-22 is stabilized by a gravity gradient boom. The boom defines the spacecraft Z axis, which is the axis of the spacecraft spin.

A final example of telemetry analysis arises from the surveys of solar array current. Detailed inspection of the data (Figure 7.20) shows that one of the solar panels, -Y, is different. It consistently produces less current, and shows different thermal characteristics.

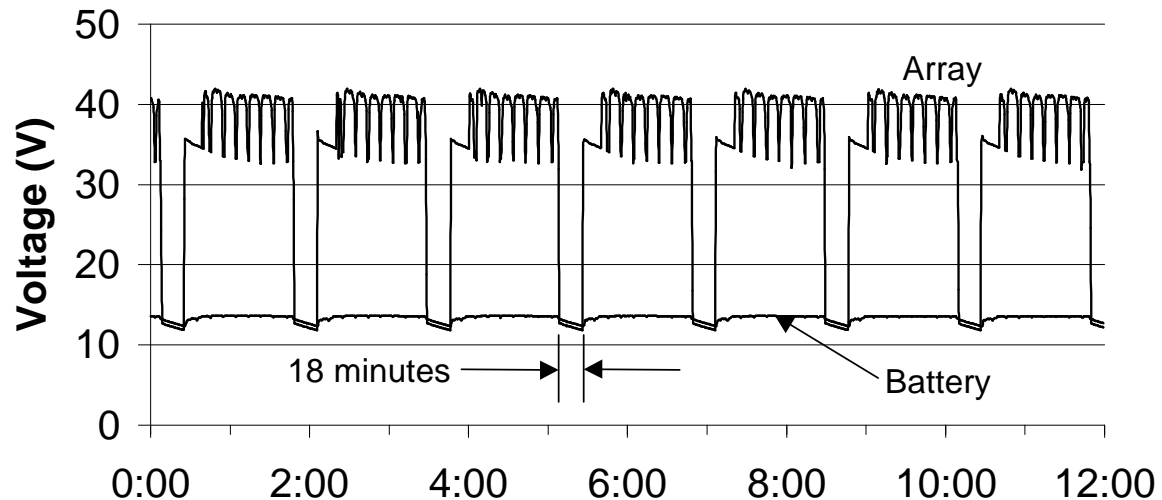


Figure 7.15: UO-22 solar array and battery voltages: 0000–1159 UTC 26 November 1999

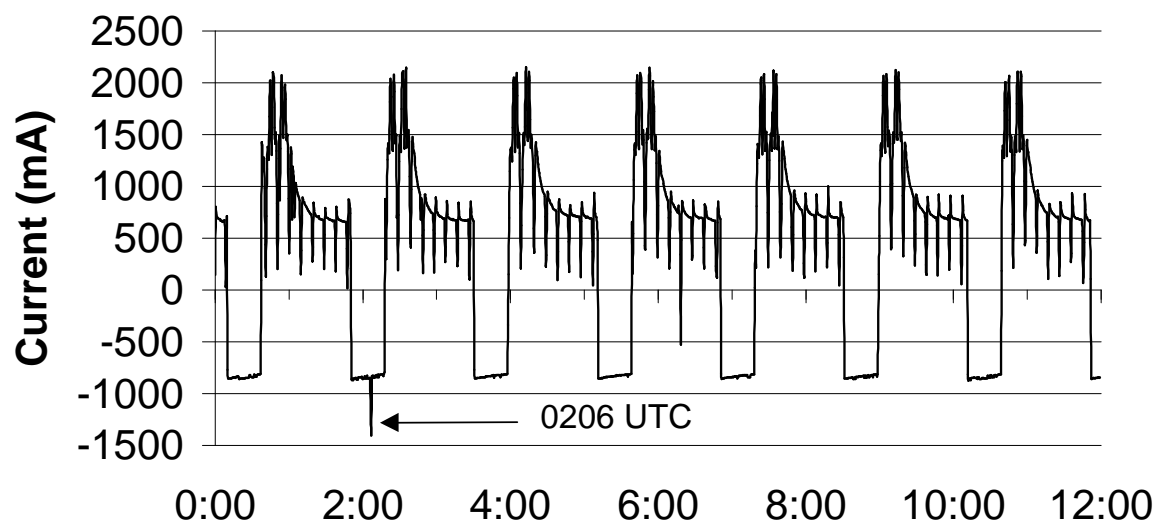


Figure 7.16: UO-22 battery current: 0000–1159 UTC 6 July 1999

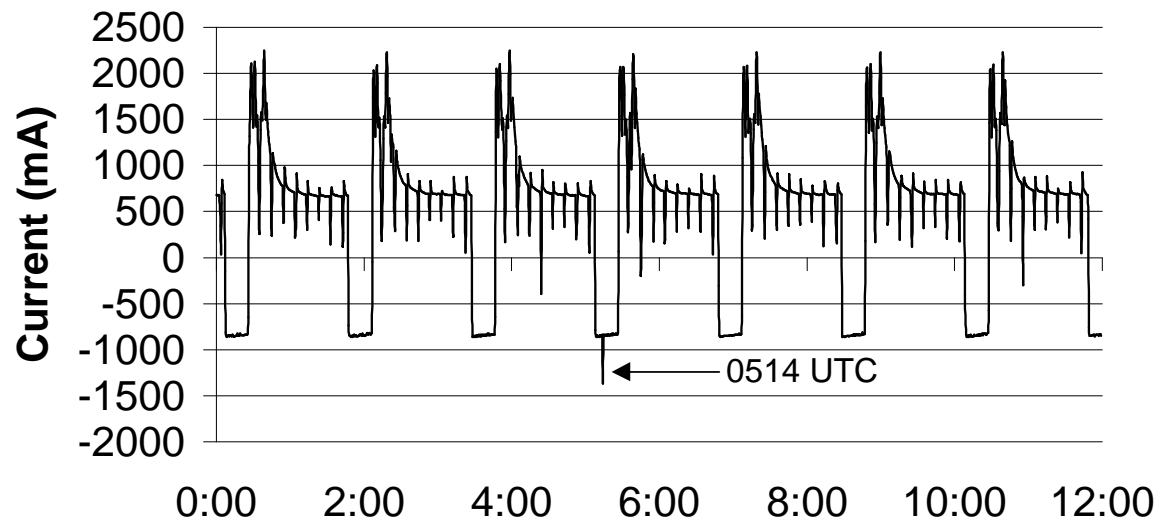


Figure 7.17: UO-22 battery current: 0000–1159 UTC 26 November 1999

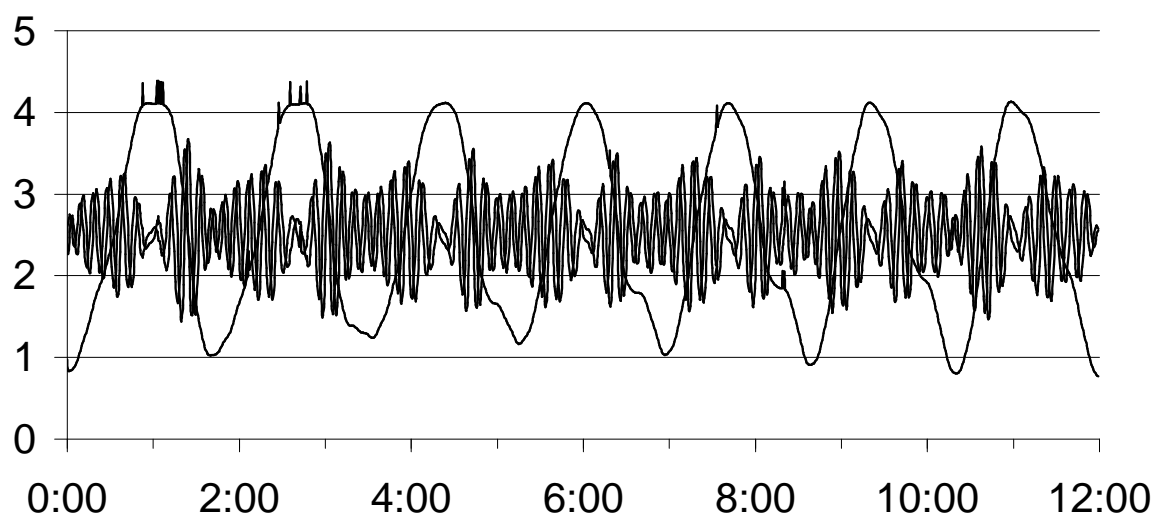


Figure 7.18: UO-22 magnetometers: 0000–1159 UTC 6 July 1999

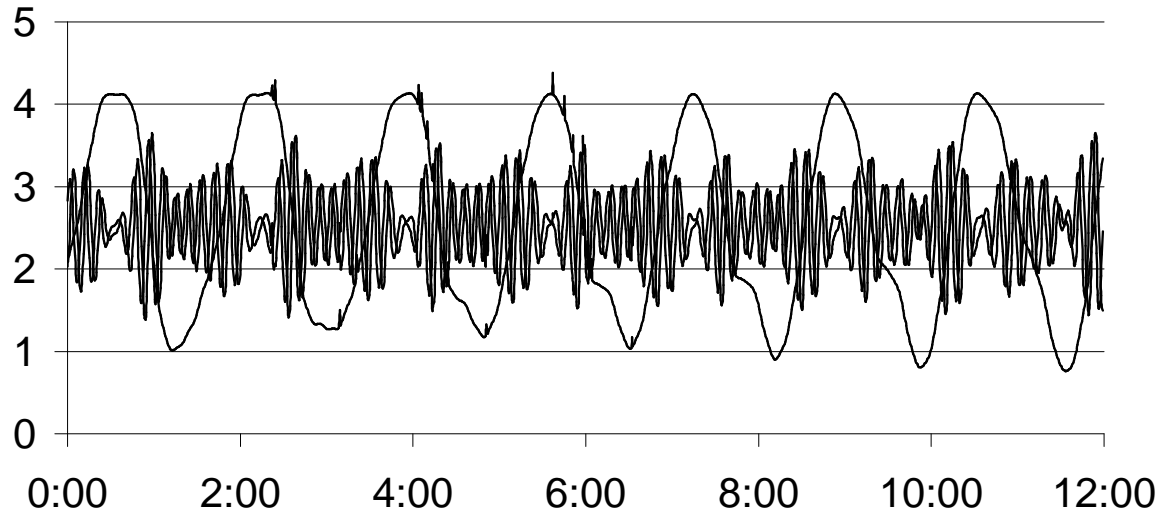


Figure 7.19: UO-22 magnetometers: 0000–1159 UTC 26 November 1999

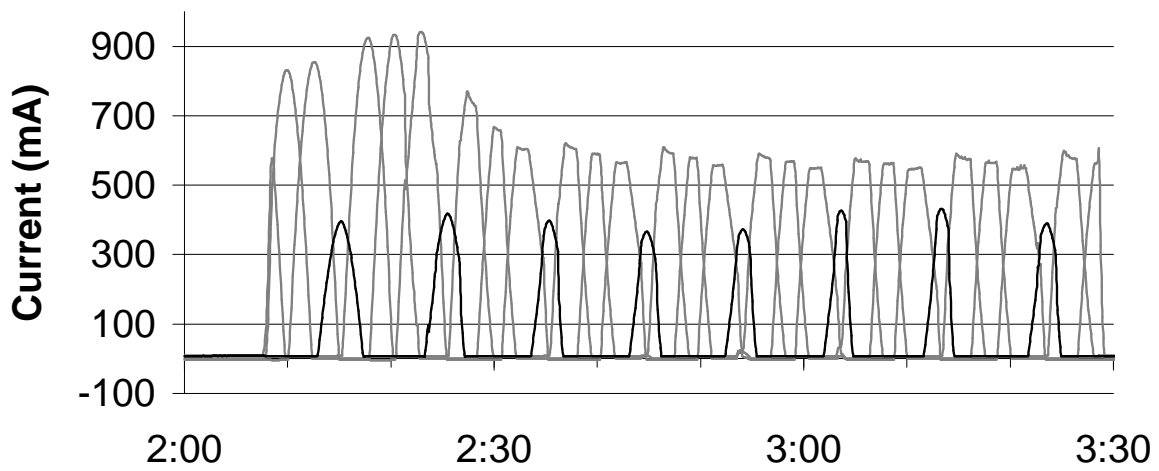
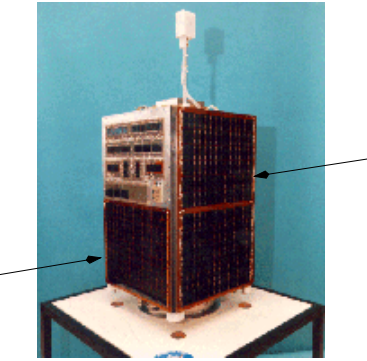


Figure 7.20: UO-22 solar array current: 0200–0330 UTC 15 July 1999

The initial hypothesis was that this panel was damaged, but inspection of a prelaunch photograph (*right*, obtained from SSTL's web site) shows that the -Y array is smaller, with the rest of that face of the satellite devoted to experiments.



Further investigation identified the experiment on UO-22 as an evaluation of solar cell technology, evaluating samples of several different GaAs, InP and Si solar cells (5).

7.4.3 Whole orbit data: AO-16

AO-16 uses an unusual system for gathering whole orbit data, as discussed in Section 4.3.4. A whole-orbit data survey was received and processed at VA3SFL on 12 October 1999. It illustrates the function of the power system and the satellite's simple stabilization system.

The plot of current from the X and Y axis solar arrays, Figure 7.21, shows the spin of the spacecraft as each array sweeps past the sun. Published references describe the use of the 2 meter antenna as a radiometer to spin the spacecraft (6). The data from the X and Y axis solar arrays show a rotation period of approximately 3 minutes. This correlates with observed ground station performance, where the spacecraft signal strength is subject to deep fades every 2 to 3 minutes.

AO-16 achieves Z axis stabilization with magnets that align the spacecraft with the Earth's magnetic field. While the data in Figure 7.22 are incomplete, they are highly suggestive of the spacecraft rotating twice around the Z axis each orbit: every 50 minutes for an orbital period of 100 minutes.

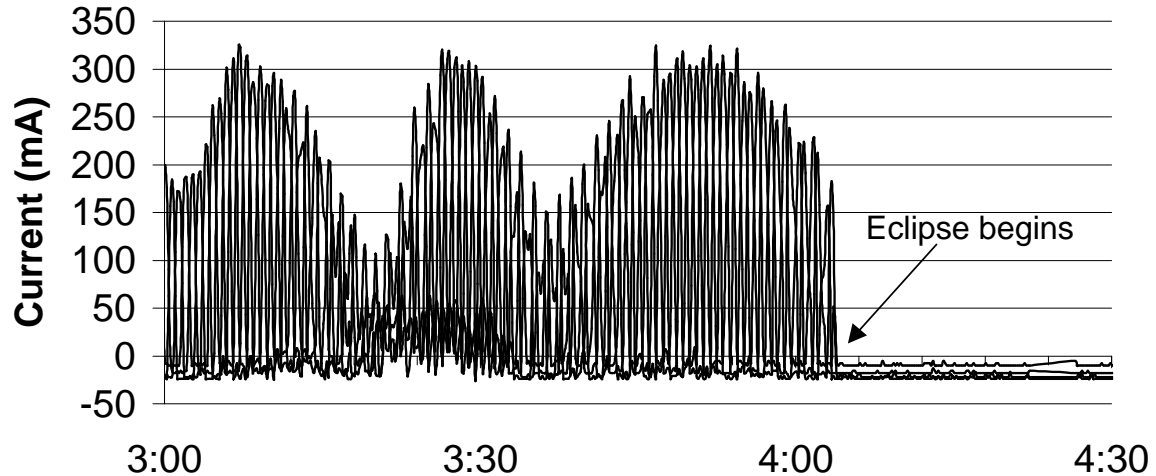


Figure 7.21: AO-16 X and Y axis solar array current: 0300–0430 UTC 12 October 1999

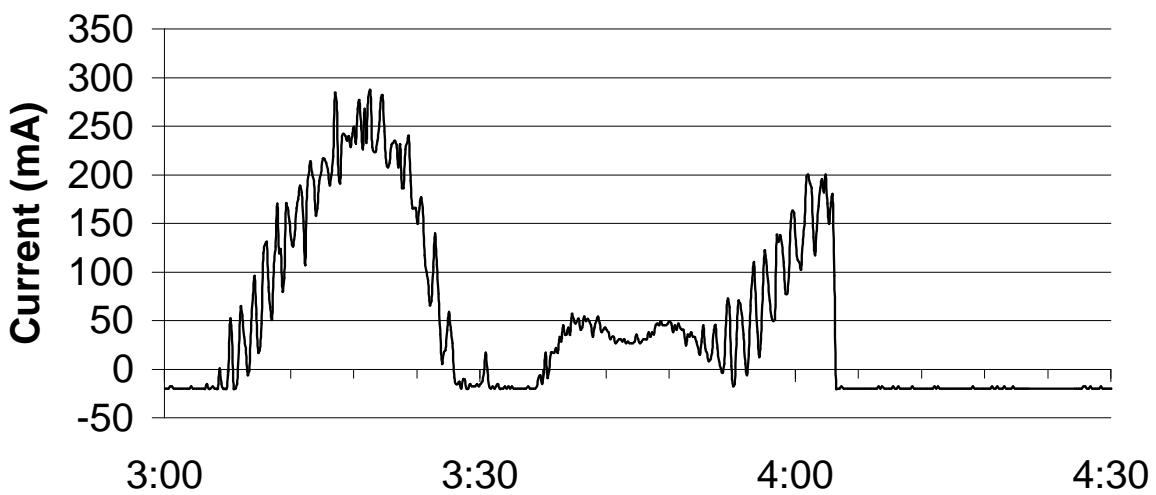


Figure 7.22: AO-16 Z axis solar array current: 0300–0430 UTC 12 October 1999

7.5 Other data analysis

Other data gathered during satellite passes were analyzed. The results from analysis of selected log files and task messages are presented.

7.5.1 Log files

Applications on board satellites create log files of their activities. Sample activity and callsign log files were downloaded from UO-22, decoded with software supplied by SSTL, and their contents analyzed.

The activity log file records FTL0 file activity and server housekeeping. An example sequence shows VK2XGJ, Wollongong NSW, Australia, uploading a file:

```
09:44:30 LOGIN      VK2XGJ-0  0 013033
09:44:31 UPLOAD     VK2XGJ-0      f#6d346 off:0 l#11413
09:45:14 UL DONE    VK2XGJ-0      11413 bytes 0 seconds
                           cksum Ack'd
                           Av upload rate 265bps
09:45:15 LOGOUT    VK2XGJ-0      013033 user disconnect
```

Another entry in the activity log shows CX5AE, Montevideo, Uruguay starting to upload a file, stopping (possibly due to LOS, **Loss Of Signal**), timing out, and being automatically logged out by the server.

```
00:55:44 LOGIN      CX5AE-0  0 012773
00:55:46 UPLOAD     CX5AE-0      f#6d2a8 off:0 l#1958
00:57:12 BLOWOFF   CX5AE-0      Inactivity timeout
00:57:38 LOGOUT    CX5AE-0      012773 server disconnect
```

The callsign log file records the callsign of every station making a request of the file server. Callsign files for 18 and 19 July 1999 were downloaded and analyzed. As expected in Figure 7.23, industrial countries were heavily over-represented with 20% of the countries (7 out of 34) accounting for 67% of the callsigns (145 out of 217). By number of callsigns the largest single user was the U.S.A.

with 49 callsigns, followed by France with 22 callsigns and Germany with 18 callsigns. During the sample period the satellite was accessed by 10 Canadian callsigns.

Asia is almost entirely represented by Japanese callsigns. The only African callsigns were from South Africa.

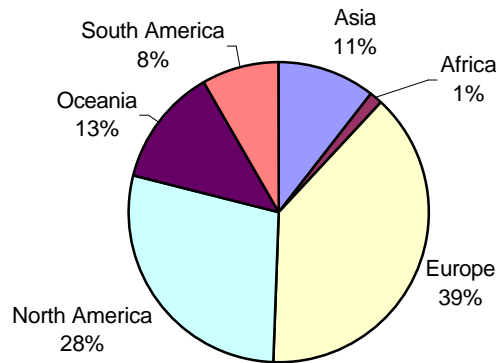


Figure 7.23: UO-22 callsigns by continent

7.5.2 Task messages

In addition to file transfer and telemetry, satellites transmit *task messages*, transmitting information relevant to various subsystems (7).

The first task message is produced by the main housekeeping task. On AO-16 it is called PHT:

```
PHT: uptime is 1910/19:36:23. Time is Sun Dec 12 01:19:57 1999
```

Note the remarkable value for uptime: AO-16 ran for over 5 years before a software crash shortly after this message was received.

A similar message received from UO-22 provides similar information. The short up time is due to reloading UO-22's software in mid-November 1999.

```
Fri Dec 17 14:32:10 1999 Up: 27/22:8 EDAC=103 F:146768
L:146016 d:1 [0].
```

Of particular interest is the EDAC number, a count of the number of error events detected by the error-correcting spacecraft memory. The F and L parameters specify the amount of free memory in SCOS and the size of the largest block of free memory, respectively.

Another task message is from the task scheduler, informing ground stations of the next scheduled operation:

```
Sked 1.5 File1:6f59a Next:Sat Dec 18 00:00:00 1999
```

The OAK attitude control system transmits valuable information:

```
OAK E:1 M:0 C:1 R:64 P:-25 Y:1133 YR:599 OX:195  
OY:-196 OZ:66 TX:0 TY:0 TZ:0
```

Of particular interest are the R, P and Y values, roll, pitch and yaw, respectively. The satellite spins, so the yaw value is always changing. The YR yaw rate parameter specifies the rate of this change. The angular parameters are in .01 degree increments, showing sub-1 degree pointing accuracy from the attitude control system which is based on a gravity-gradient boom and magnetorquers.

Not all task messages are as well documented. The following task message was received from KO-25 and is probably from the Earth Imaging System, but the significance of the individual values is unknown:

```
EIS:<385a70d9> [s4] Timer:0 TxEnable:1
```

7.6 Performance analysis

The downlink performance of UO-22 and TO-31 was analyzed. Particular emphasis was placed on protocol overhead and effective throughput, and the results are presented here.

7.6.1 Environmental issues

The environment in which the ground station operates was analyzed.

The present ground station antennas are on the roof of the UTIAS building in Downsview, Ontario. The area is flat, part of southern Ontario on the north shore of Lake Ontario. There are thus no geographic obstacles. While there are deciduous trees, they subtend an angle of less than 5 degrees as seen from the ground station antenna site, and had no discernable effect on ground station performance. In both summer and winter 435 MHz signals from satellites were acquired within seconds of theoretical AOS (Acquisition Of Signal), and lost within seconds of theoretical LOS. No seasonal effects were noted between July and December.

The only detectable obstruction was the satellite television antenna on the roof of the UTIAS building. This attenuated signals for a satellite azimuth from approximately 200 to 240 degrees, at elevation angles below 15 degrees. This is a small part of the sky, and the loss of data is minimal. Such an environment would not affect MOST, since passes in the southwest have mutual visibility with the proposed ground station in Vancouver.

7.6.2 Data throughput

Data were gathered during a representative week, 22 to 26 July 1999, to evaluate access time, net data throughput, and the amount of data transferred. The ground station operations were nominal, as were the satellite operations.

The first measurement was access time. As shown in Figure 7.24, the access time is uniform over the study period. Minor variations are mainly due to orbital geometry and average out over longer periods.

The amount of data transferred was then computed. Protocol information was analyzed with an instrumented version of decode (Appendix C) that classified packets by their function and tallied the number of bytes devoted to file transfer. This compensated for the multiplexed nature of the

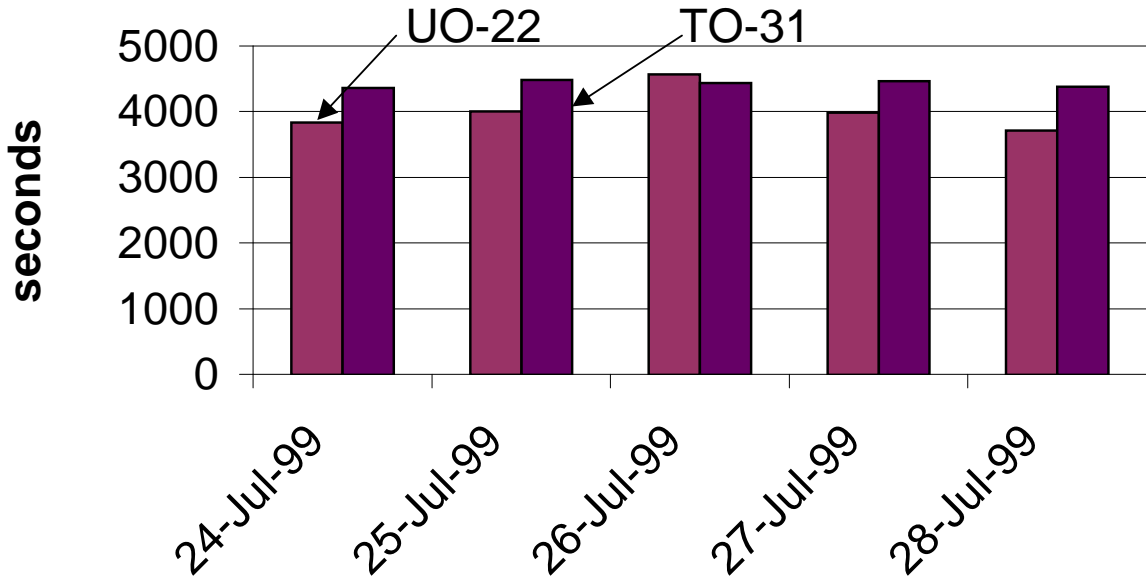


Figure 7.24: UO-22 and TO-31 access time, 22–26 July 1999

downlink—rather than counting the bytes received at VA3SFL, the count was of all bytes transmitted by the satellite, more closely approximating the environment anticipated for MOST.

The final analysis combines the results of Figures 7.24 and 7.25 to determine the net number of bytes per second transferred from the satellite, as presented in Figure 7.26. TO-31 has consistently shown higher throughput, believed to be partially the result of a higher duty cycle on its downlink, and partially the result of lower protocol overhead (Section 7.6.3). In November 1999 this duty cycle was increased, with many passes showing throughput exceeding 1000 bytes per second. Reliability concerns with the ground station (Section 7.3.4) have precluded further analysis of this development.

7.6.3 Protocol overhead

Protocol overhead was analyzed with an instrumented version of `decode` (Appendix C) that classified packets by their function and tallied the number of bytes. All data received on the downlink for the week of 20 July 1999 were used for the analysis.

Differences were observed, as reported in Figures 7.27 and 7.28. UO-22 transfers large numbers of small files, and thus must devote more of its downlink to directory information. TO-31 transfers small numbers of large files, and can thus devote more downlink capacity to actually transferring files.

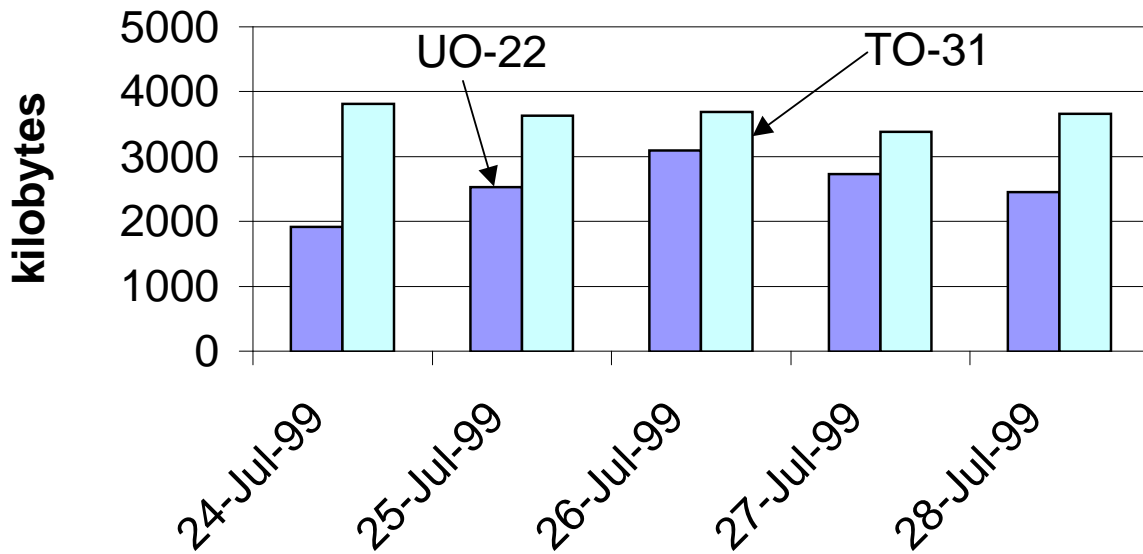


Figure 7.25: UO-22 and TO-31 file transfer, 22–26 July 1999

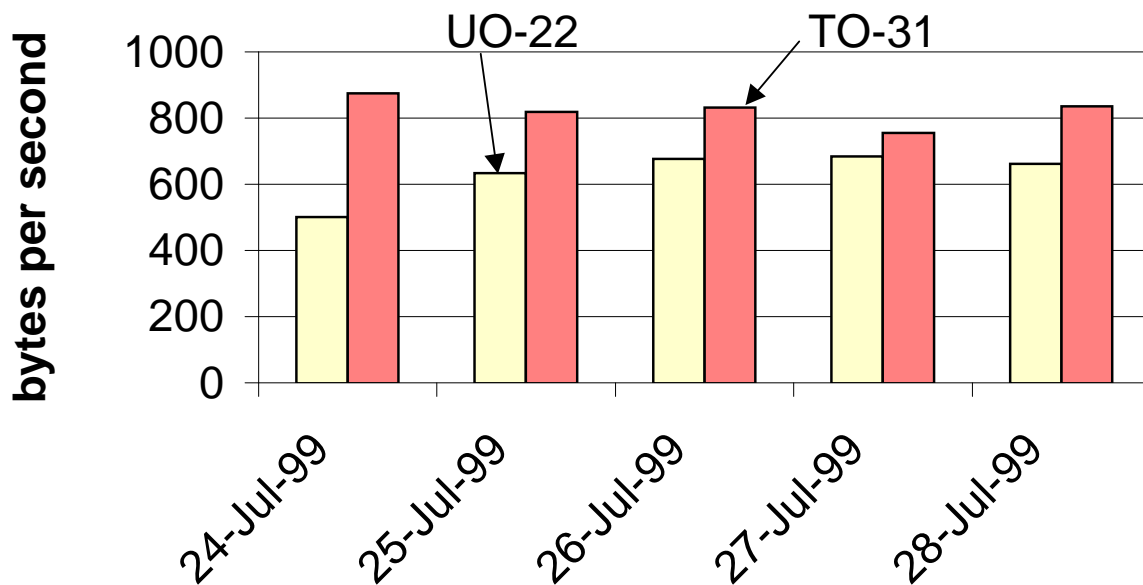


Figure 7.26: UO-22 and TO-31 throughput, 22–26 July 1999

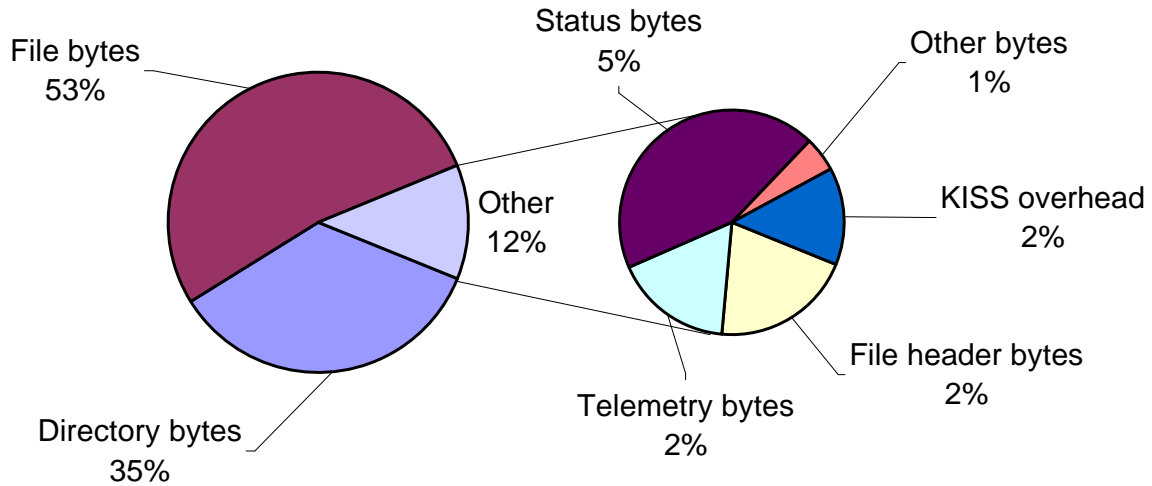


Figure 7.27: UO-22 protocol overhead analysis: July 1999

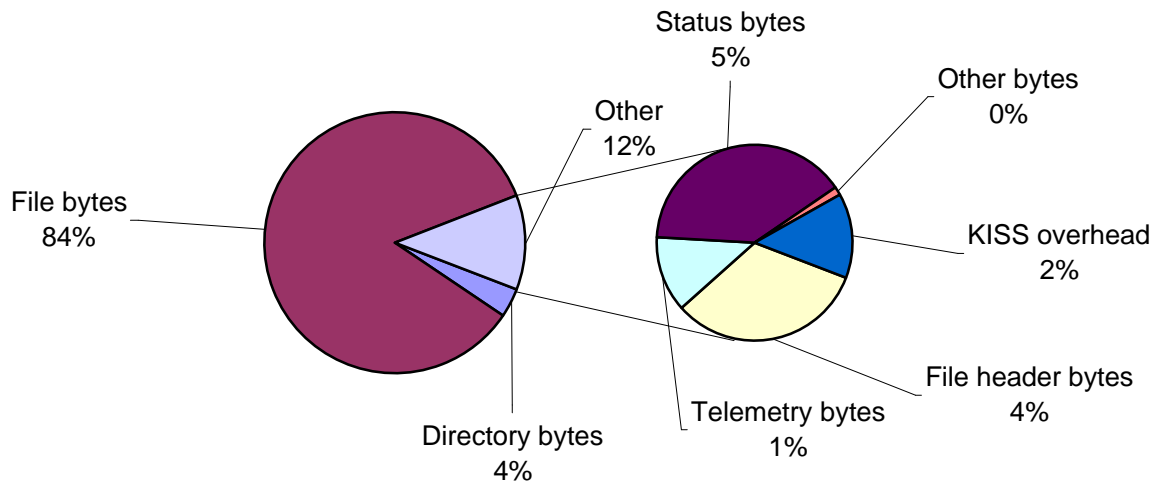


Figure 7.28: TO-31 protocol overhead analysis: July 1999

7.9 Notes and references

1. Geological Survey of Canada. *Canadian Geomagnetic Reference Field, 1998*.
Internet: http://www.geolab.nrcan.gc.ca/geomag/e_crgf.html
2. J. White and R. Haighton, AMSAT-NA, personal communication.
3. C. Jackson, SSTL, personal communication.
4. W. Larson and J. Wertz, editors, *Space Mission Analysis and Design, 2nd edition*. Torrance: Microcosm and Dordrecht: Kluwer Academic Publishers, 1992.
5. M. Sweeting, “UoSAT microsatellite missions” in *Electronics & Communication Engineering Journal*, June 1992. Figure 11 is a closeup view of this experiment.
6. M. Davidoff, *The Radio Amateur’s Satellite Handbook*. Newington: ARRL, 1998.
7. C. Jackson, “UoSAT Spacecraft Operation”, paper presented at the 11th AMSAT-UK Colloquium, 1996.
Internet: <http://www.ee.surrey.ac.uk/CSER/UOSAT/amateur/taskinfo.html>
8. A. Ward, “Low noise Amplifiers for 2304, 3456, 5760 and 10368 MHz using the ATF-36077 PHEMT” in *Proceedings of Microwave Update ’97*. Newington: ARRL, 1997.
9. G. Hoch, “Yagi Versus Aperture Antennas” in *The ARRL UHF/Microwave Experiemnter’s Manual*. Newington: ARRL, 1990.
10. W. Vogel and J. Goldhirsh, “Multipath fading at L band for low elevation angle, land mobile satellite scenarios” in *IEEE Journal on Selected Areas in Communications*, vol. SAC-13:2, February 1995.
11. J. Goldhirsh and W. Vogel, “Mobile satellite system fade statistics for shadowing and multipath from roadside trees at UHF and L band” in *IEEE Transactions on Antennas and Propagation*, vol. AP-37:4, April 1989.
12. H. Smith et al, “Characterisation of the high elevation orbit satellite-mobile radio channel at L and S bands” in *IEE Colloquium on Land Mobile Satellite Systems*, 1992.